Supporting information

Anion-Dependent Molecular Doping and Charge Transport in Ferric Salts Doped P3HT for Thermoelectric Application

Lili Wu,[†,‡] Hui Li,[,†,‡] Haoyu Chai,[†,§] Qing Xu,[†,‡,#] Yanling Chen,[†,‡,#] Lidong Chen[*,†,‡]*

[†]State Key Laboratory of High Performance Ceramics and Superfine Microstructure, Shanghai Institute of Ceramics, Chinese Academy of Sciences, Shanghai 200050, China.

[‡]Center of Materials Science and Optoelectronics Engineering, University of Chinese Academy of Sciences, Beijing 100049, China

[§]School of Materials Science and Engineering, Jingdezhen Ceramic Institute, Jingdezhen 333001, China

[#]School of Physical Science and Technology, ShanghaiTech University, Shanghai 201210, China

*Corresponding author

*E-mail: lihui889@mail.sic.ac.cn

*E-mail: cld@mail.sic.ac.cn

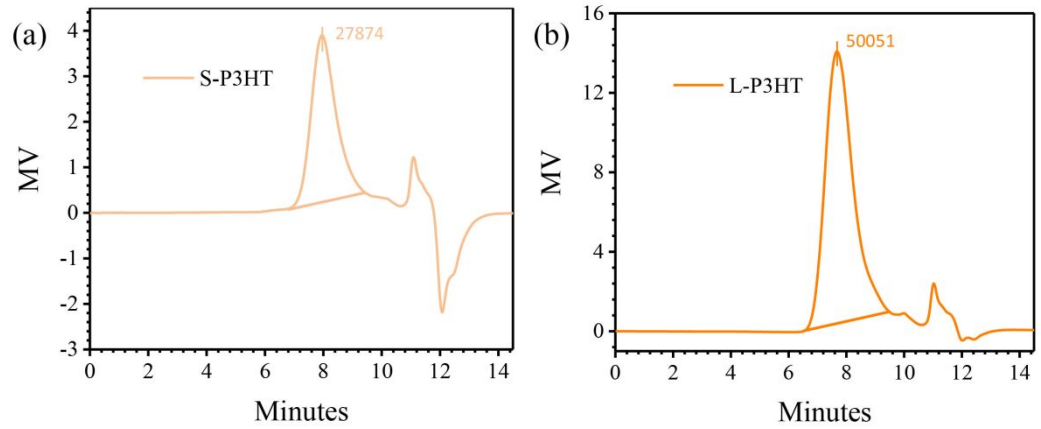

Figure S1. Gel permeation chromatography (GPC) images for (a) the S-P3HT (M_n=14.52 kDa) and (b) the L-P3HT (M_n=25.12 kDa).

Table S1. Molecular weight data of S-P3HT and L-P3HT.

Sample	M_n (Da)	M_w (Da)	M_p (Da)	Polydispersity Index
S-P3HT	14515	31592	27874	2.18
L-P3HT	25117	60256	50051	2.40

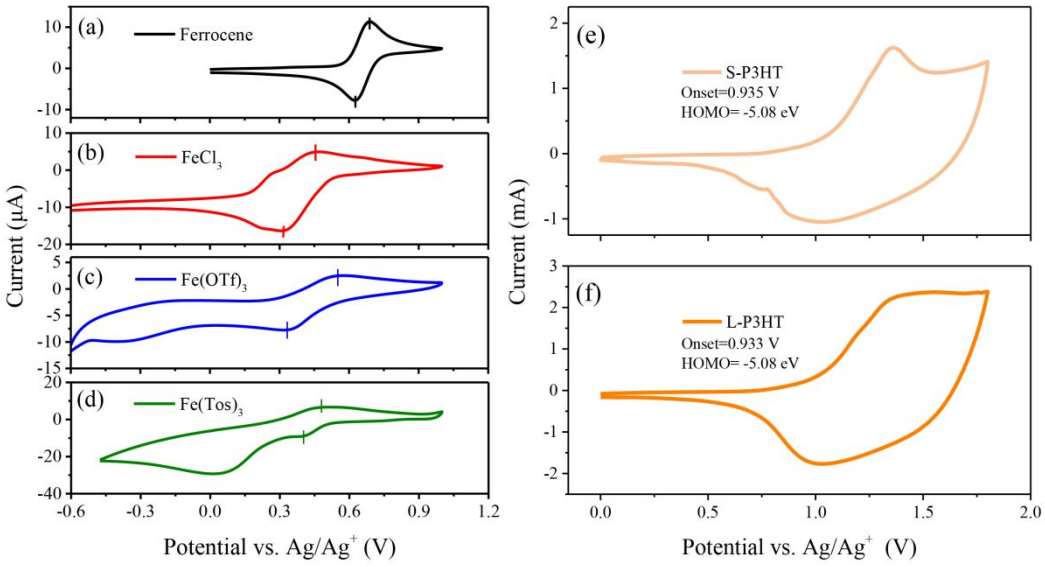

Figure S2. Cyclic Voltammetry of ferrocene (a), ferric salt dopants (b-d) and P3HT (e

and f) (Fc/Fc^+ as external calibration). Scan rate is 0.1 $V \cdot s^{-1}$.

The calculation process of energy level:

For calibration, the redox potential of Fc/Fc^+ was measured under the same conditions, and it is located at 0.65 V to the Ag/Ag^+ electrode. It is assumed that the redox potential of Fc/Fc^+ has an absolute energy level of -4.80 eV to vacuum (Adv. Mater., 2011, 23, 2367-2371). For P3HT, polymer solution was deposited onto the working electrode and form continuous film. The oxidation potentials are estimated by the onset potential: HOMO = $-e(E_{ox\ vs.\ Fc/Fc+} + 4.15)$ (eV). For dopants, bare working electrode was immersed in dopant solution. The half-wave potentials ($E_{1/2}$) were used to calculate LUMO levels: LUMO = $-e(E_{1/2\ vs.\ Fc/Fc+} + 4.15)$ (eV).

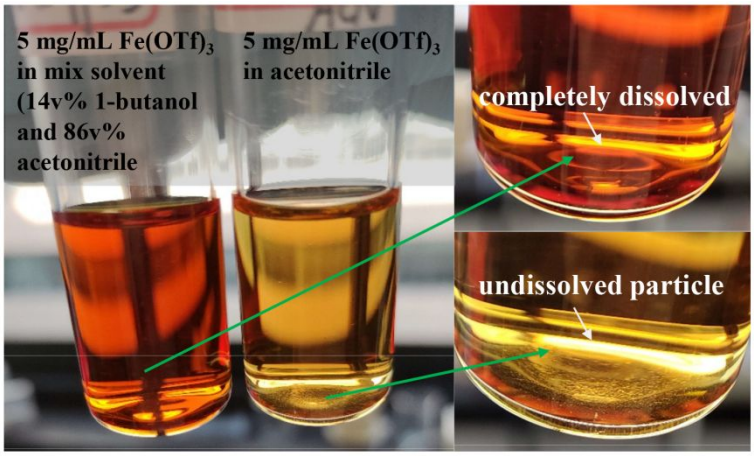

Figure S3. Better solubility of $Fe(OTf)_3$ in a mixed solvent compared with in pure acetonitrile.

Table S2. The integrated area ratio of two bands for undoped and doped P3HT with different M_n.

Sample	$Band_I$ (320~700nm)	$Band_{II}$ (700~2500 nm)	$R = Band_{II}/Band_I$
S-pristine	224	43	0.19
S-$FeCl_3$	109	316	2.90
S-$Fe(OTf)_3$	176	868	4.93
S-$Fe(Tos)_3$	165	233	1.41
L-pristine	192	16	0.08
L-$FeCl_3$	155	374	2.41
L-$Fe(OTf)_3$	141	784	5.56
L-$Fe(Tos)_3$	180	110	0.61

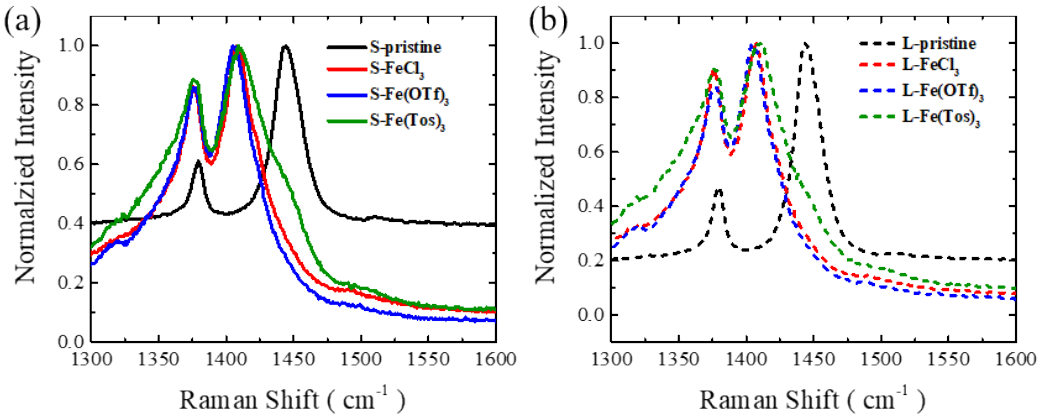

Figure S4. Raman spectra of (a) pristine P3HT, $FeCl_3$-doped P3HT, $Fe(OTf)_3$-doped P3HT, and $Fe(Tos)_3$-doped P3HT with M_n=14.52 kDa. (b) Pristine P3HT, $FeCl_3$-doped P3HT, $Fe(OTf)_3$-doped P3HT, and $Fe(Tos)_3$-doped P3HT with M_n = 25.12 kDa.

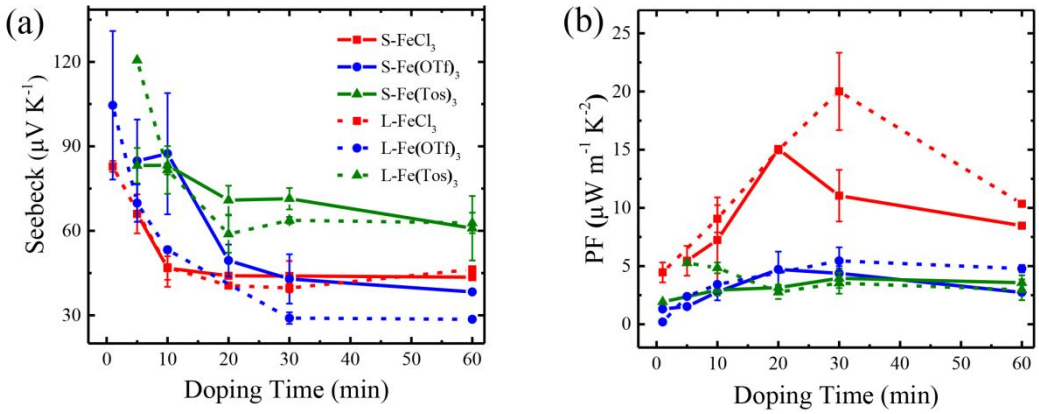

Figure S5. (a) Seebeck coefficient of doped P3HT. (b) Power factor of doped P3HT with different M_n.

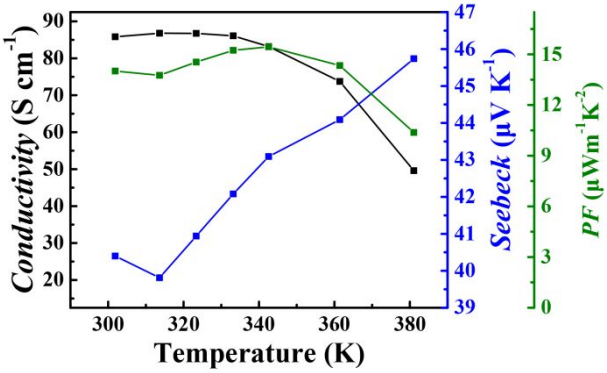

Figure S6. Temperature-dependent electrical conductivity, Seebeck coefficient and power factor for $FeCl_3$-doped L-P3HT. (The TE performance was tested after the sample was stored in the glovebox for one month)

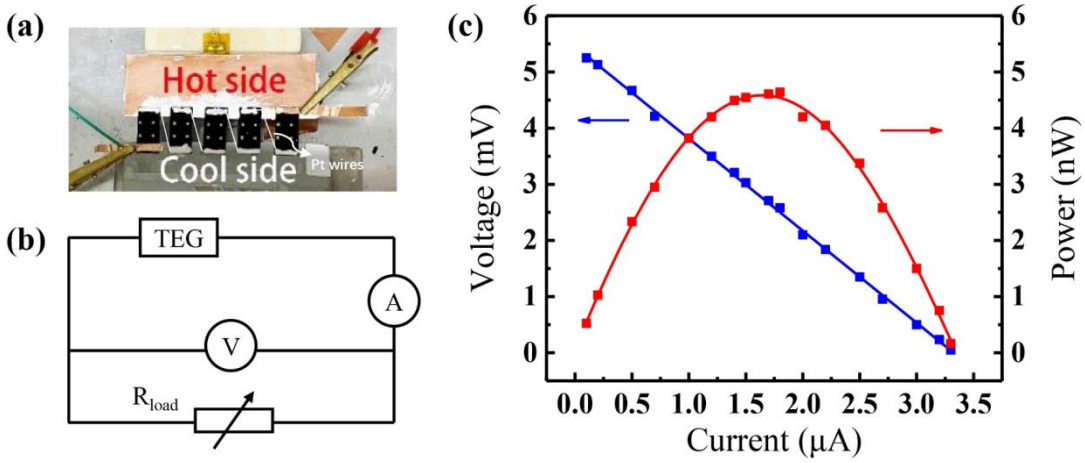

Figure S7. (a) Schematic illustration of a 5-legged TE module based on $FeCl_3$-doped L-P3HT. (b) Illustration of thermoelectric performance measurement of the TE module. (c) Output voltage and output power as a function of current at a temperature difference of 23.3 K.

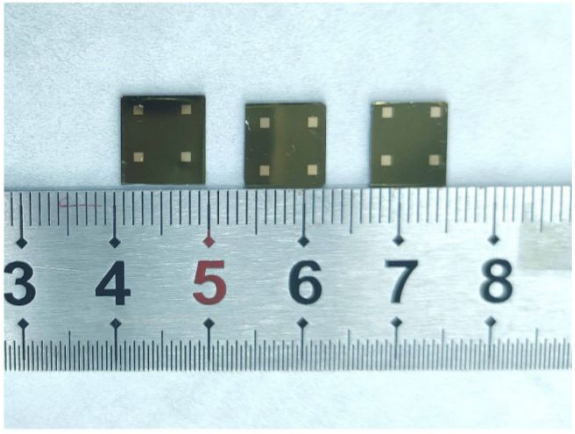

Figure S8. The photograph of prepared samples with Van der Pauw geometries for AC-Hall effect measurement.

Table S3. The electrical conductivities, mobility and carrier concentration of L-P3HT doped by $FeCl_3$ and $Fe(OTf)_3$, respectively, determined by AC-Hall effect measurement by using van der Pauw measurement method. (The samples for electrical conductivity measurements were cut into square size and then used for Hall experiments. All data are extracted from three devices. The electrical conductivity tested by LakeShore was lower than that of ZEM results probably due to the degradation during experimental preparation. Nevertheless, the σ of $FeCl_3$-doped P3HT is still two times higher than that of $Fe(OTf)_3$-doped P3HT)

Sample	σ (S cm^{-1})	n (10^{21} cm^{-3})	μ_H (cm^2 V^{-1} s^{-1})
L-$FeCl_3$	94.9±2.4	1.8±0.1	0.31±0.01
L-$Fe(OTf)_3$	34.9±1.8	2.1±0.1	0.10± 0.01

Table S4. The lamellar distance extracted from out-of-plane pattern and π-π stacking distance extracted from in-plane pattern. FWHM was calculated from the first-order diffraction peak of (100).

Sample	lamellar distance (Å)	π-π stacking distance (Å)	FWHM (Å^{-1})
S-pristine	16.59	3.79	0.046
S-$FeCl_3$	18.12	3.59	0.040
S-$Fe(OTf)_3$	18.44	3.55	0.038
S-$Fe(Tos)_3$	17.66	3.69	0.053
L-pristine	16.41	3.77	0.042
L-$FeCl_3$	18.01	3.59	0.039
L-$Fe(OTf)_3$	18.66	3.53	0.037
L-$Fe(Tos)_3$	18.07	3.61	0.050

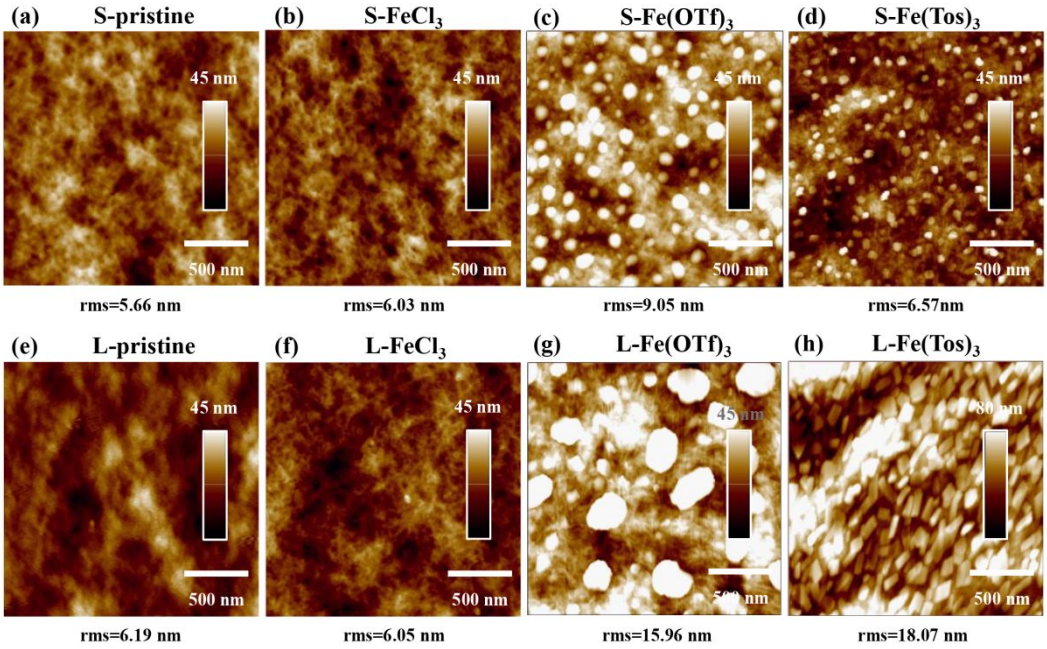

Figure S9. AFM images for undoped and doped P3HT with different M_n.